Strong discontinuity modeling of cracking in concrete

J. Oliver, E. Samaniego, E. Chaves
ETS Enginyers de Camins, Canals i Ports de Barcelona, Technical University of Catalonia (UPC),
Campus Nord UPC, Edifici C-1, C/Jordi Girona 1-3
08034 Barcelona, Spain

A. Huespe
CIMEC -Conicet-Unl
Instituto Intec, Guemes 3450
3000 Santa Fe, Argentina

ABSTRACT: The ingredients to model the onset and development of cracking, in plain or reinforced concrete, in a strong discontinuity scenario are given. After describing the analytical foundations of the strong discontinuity approach (SDA), such as the strong discontinuity kinematics, softening regularization and the discontinuous bifurcation analysis, numerical issues like finite elements with embedded discontinuities and propagation algorithms are presented. A viscous perturbation based algorithm, to unfold bifurcations due to simultaneous crack arrest/activation for multiple crack cases, is described as well. Numerical examples show the performance of the presented methodology.

1 CRACK MODELING IN A STRONG DISCONTINUITY SETTING

1.1 *The strong discontinuity approach to Fracture Mechanics*

The strong discontinuity approach (see Oliver et al. 2001 for an overview) appears as an alternative to discrete fracture mechanics (Bazant & Planas 1998) to model the onset and development of cracks at quasibrittle fracturing media. The main features of the approach are the following:

1. The use of a *continuum format* for the kinematics i.e.: the strains $\boldsymbol{\varepsilon}(\mathbf{x})$ are computed as the symmetric gradient of the displacement field $\mathbf{u}(\mathbf{x})$, even when $\mathbf{u}$ exhibits jumps across the crack path and, therefore, $\boldsymbol{\varepsilon}(\mathbf{x})$ becomes unbounded (see Figure 1). The displacement and strain fields read:

$$\mathbf{u}(\mathbf{x}) = \bar{\mathbf{u}}(\mathbf{x}) + H_S [\![\mathbf{u}]\!](\mathbf{x})$$

$$\boldsymbol{\varepsilon} = \nabla^s \mathbf{u} = \underbrace{\bar{\boldsymbol{\varepsilon}}}_{\substack{regular \\ (bounded)}} + \underbrace{\delta_S ([\![\mathbf{u}]\!] \otimes \mathbf{n})^S}_{singular\,(unbounded)} \qquad (1)$$

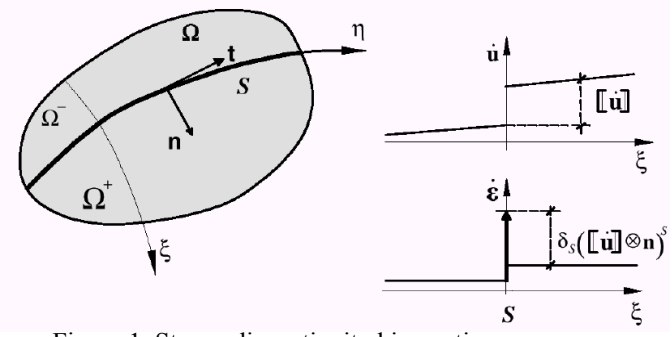

Figure 1. Strong discontinuity kinematics

where H_S and δ_S stand, respectively, for line/surface Heaviside's step function and Dirac's delta function placed on the discontinuity path S in the body Ω, $\bar{\mathbf{u}}(\mathbf{x})$ is the regular (continuous) displacement field, $[\![\mathbf{u}]\!](\mathbf{x})$ is the displacement jump and $\mathbf{n}(\mathbf{x})$ is the unit normal to the discontinuity path S. This is known in the literature as *strong discontinuity kinematics* (Simo, Oliver & Armero 1993).

2. Consideration of standard (continuum stress-strain) rate-independent non-linear constitutive equations equipped with strain softening i.e.:

$$\boldsymbol{\sigma} = \boldsymbol{\Sigma}(\boldsymbol{\varepsilon}, H) \qquad (2)$$

where $H \le 0$ stands for *the continuum softening modulus* that rules the evolution of the elastic domain. The rate version of equation (2) reads:

$$\dot{\boldsymbol{\sigma}} = \mathbb{C}^{tang}(\boldsymbol{\sigma}, H) : \dot{\boldsymbol{\varepsilon}}, \qquad (3)$$

where $\mathbb{C}^{tang}$ is the tangent constitutive tensor.

3. The distributional character of the inverse of the *continuum* softening modulus H in terms of the *discrete* softening modulus $\bar{H}$ (which can be related to the fracture properties of the material) i.e.:

$$\frac{1}{H} = \delta_S \frac{1}{\bar{H}} \qquad (4)$$

Regularized versions (more suitable for computational treatments) of equations (1) and (4) are obtained via a k-regularized sequence of Dirac's delta functions:

$$\delta_S(\mathbf{x}) \equiv \lim_{k\to o} \frac{\mu_S(\mathbf{x})}{k} \tag{5}$$

where $\mu_S(\mathbf{x})$ is the collocation function on S ($\mu_S(\mathbf{x})=1$ for $\mathbf{x}\in S$; $\mu_S(\mathbf{x})=0$ otherwise) and k is a regularization parameter as small as permitted by the machine precision. In this context equation (4) turns out to be the so-called *softening regularization condition* (Oliver 2000):

$$\begin{aligned} &H = k\overline{H} \quad \forall \mathbf{x}\in S \\ &H = \infty \quad \text{otherwise (elastic unloading)} \end{aligned} \tag{6}$$

Under those conditions it can be shown (Oliver 2000) that:

a) Equation (4) makes compatible, for the constitutive equation (2), bounded values of the stresses $\boldsymbol{\sigma}$ with the unbounded strains emerging from equation (1) at the discontinuity interface S.
b) As the strong discontinuity kinematics (1) is activated, the original continuum constitutive equation (2) is projected into *a discrete constitutive model* (relating the traction $\boldsymbol{\mathcal{T}} = \boldsymbol{\sigma}\cdot\mathbf{n}$ with the jump $[\![\mathbf{u}]\!]$) that is *automatically fulfilled* at the discontinuity interface S (Oliver 2000) i.e.:

$$\boldsymbol{\mathcal{T}} = \boldsymbol{\mathcal{F}}([\![\mathbf{u}]\!], \overline{H}) \tag{7}$$

Equation (7) provides a clear link with the non-linear decohesive Fracture Mechanics (Bazant & Planas 1998) while keeping the continuum format of the analysis.

1.2 *Onset and propagation of a crack*

Failure Mechanics tools, like *the discontinuous bifurcation analysis* (Willam 2000), provide a rigorous methodology to detect the onset of a crack in a given material point $\mathbf{x}$, based on the properties of the (directional) localization tensor $\mathbb{Q}^{loc}$:

$$\mathbb{Q}^{loc}(\mathbf{x},\mathbf{n},t) = \mathbf{n}\cdot\mathbb{C}^{tang}(\boldsymbol{\sigma}(\mathbf{x},t), H)\cdot\mathbf{n} \tag{8}$$

The singularity of $\mathbb{Q}^{loc}$ can be shown to be associated to the appearance of a discontinuous bifurcation of the stress/strain fields in the neighborhood of $\mathbf{x}$. Therefore the bifurcation time $t_B(\mathbf{x})$, that triggers the discontinuous kinematics (1), and the (normal to) propagation direction $\mathbf{n}$ (see Figure 1) are determined by the first time that the following condition is fulfilled for some $\mathbf{n}$:

$$\det(\mathbb{Q}^{loc}(\mathbf{x},\mathbf{n},t_B)) = 0 \tag{9}$$

Simplified alternatives are frequently used by associating t_B to the onset of the non-linear material behavior and $\mathbf{n}$ to the direction of the first principal stress at that time. Although less rigorous than the previous procedure, this seems to provide accurate enough results for quasibrittle materials like concrete.

1.3 *Finite element technology*

For numerical simulation purposes finite elements with embedded discontinuities, compatible with the strong discontinuity kinematics (1), are required. In the last years several families of such elements have been developed. Their common feature is that the standard underlying element is enriched with additional displacement/strain fields that make it compatible with the presence of a discontinuity embedded in the element. In this context, two different families can be distinguished:

- Elemental enrichment (see for instance Oliver 1996, Armero&Garikipati 1996).
- Nodal enrichment (see for instance Wells& Sluys 2001).

1.3.1 *Elemental enrichment*

The support of the enriching discontinuity mode is elemental (see Figure 2) and, in consequence, the additional internal discontinuous degrees of freedom (two per element in 2D cases) can be condensed at the elemental level. The displacement jump is element-wise constant.

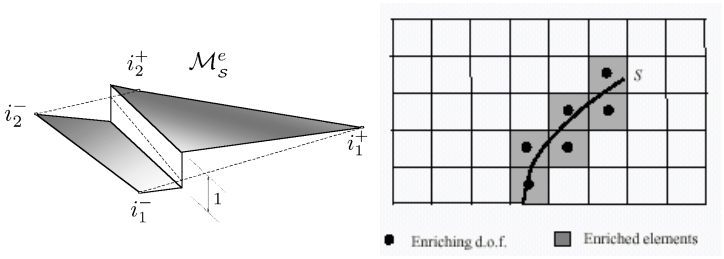

Figure 2. Elemental based enrichment. Left: discontinuous enriching displacement mode. Right: enriched domain crossed by the discontinuity path

1.3.2 *Nodal enrichment*

The support of the enriching discontinuous mode is the same than for the nodal shape functions of the underlying element (see Figure 3). The regular nodes of the enriched set of elements are increased with additional degrees of freedom (two per node in 2D cases) whose interpolation provides a (varying inside the element) discontinuous displacement field. The additional degrees of freedom can not be condensed at element level.

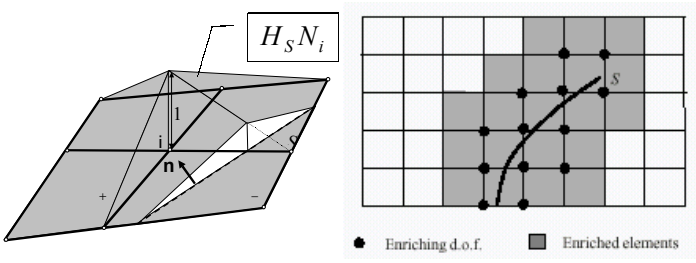

Figure 3. Nodal based discontinuous enrichment. Left: discontinuous enriching displacement mode. Right: enriched domain crossed by the discontinuity path

1.4 *Discontinuity tracking algorithms*

Constructing the additional discontinuous modes, in finite elements with embedded discontinuities discussed in section 1.3, require the definition of the set of enriched elements (see Figure 2) and the position of the discontinuity path inside every element of that set. Procedures and algorithms devoted to that purpose are termed *tracking algorithms* and can be classified into:

- *Propagation algorithms* (see Figure 4): based on the recursive propagation from the *root element* (the first to fulfill the bifurcation condition (9)) to the neighbor elements by means of element-wise straight segments (in 2D), or planes (in 3D) orthogonal to the elemental normal vector $\mathbf{n}$. Although very intuitive and direct to implement their application to multiple cracks or to 3D cases is cumbersome.

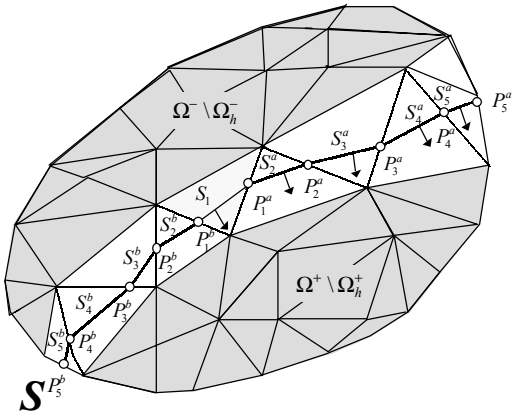

Figure 4. Discontinuity tracking in a 2D problem using a propagation algorithm:. The original segment S_1 in the root element propagates in both senses by means of straight elemental segments S_i^a and S_i^b.

- *Global tracking algorithms* (see Figure 5): They aim at tracing, *at once*, all the lines (in 2D), or surfaces (in 3D), candidates to be discontinuity paths (cracks). These lines, or surfaces, are determined as that family of curves or surfaces that are orthogonal to the vector field $\mathbf{n}(\mathbf{x})$ provided by the bifurcation condition (9). Once this family is known those lines passing through the center of a root element are selected to contain a propagating crack.

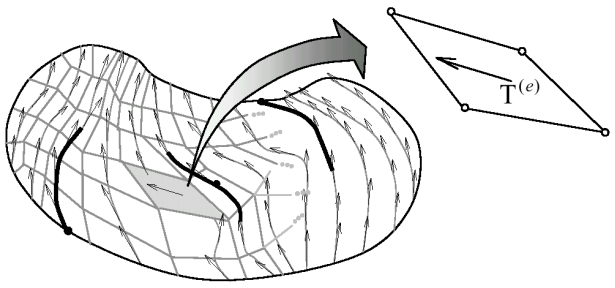

Figure 5. Discontinuity tracking in a 2D problem using a global algorithm. The algorithm traces the envelopes of the propagation vector field $\mathbf{T}(\mathbf{x}) \perp \mathbf{n}(\mathbf{x})$ and then selects some of them as propagating cracks.

In Oliver et al. (2002) a *heat conduction-like algorithm* to provide those envelopes is presented. The algorithm is based on the solution of an stationary heat conduction problem, on the same finite element mesh as for the mechanical problem, at every time step of the analysis. It is shown that considering the following, directional point dependent, conductivity tensor, $\mathbb{K}(\mathbf{x})$:

$$\mathbb{K}(\mathbf{x}) = \mathbf{T}(\mathbf{x}) \otimes \mathbf{T}(\mathbf{x}) \tag{10}$$

for 2D cases and ,

$$\mathbb{K}(\mathbf{x}) = \mathbf{S}(\mathbf{x}) \otimes \mathbf{S}(\mathbf{x}) + \mathbf{T}(\mathbf{x}) \otimes \mathbf{T}(\mathbf{x}) \tag{11}$$

for 3D cases, where $\mathbf{S}(\mathbf{x})$ and $\mathbf{T}(\mathbf{x})$ are any couple of vector fields, orthogonal to the field $\mathbf{n}(\mathbf{x})$ (which can be trivially computed) the solution of the heat conduction problem in Figure 6 provides a temperature distribution $\theta(\mathbf{x})$ whose isolines are the intended envelopes. In order to avoid either a singular problem or a trivial (constant temperature) solution, arbitrary, and different, values of the temperatures should be prescribed at two points of the continuum.

$$FIND: \theta(\mathbf{x}) \qquad \text{satisfying:}$$

$$\nabla \cdot \mathbf{q} = 0 \qquad in\ \Omega$$

$$\mathbf{q} = -\mathbb{K} \cdot \nabla\theta = -\mathbf{T}\frac{\partial\theta}{\partial T} \qquad in\ \Omega$$

$$\mathbf{q} \cdot \nu = (\nu \cdot \mathbf{T})\frac{\partial\theta}{\partial T} = 0 \qquad on\ \partial_q\Omega$$

$$\theta = \theta^* \qquad on\ \partial_\theta\Omega$$

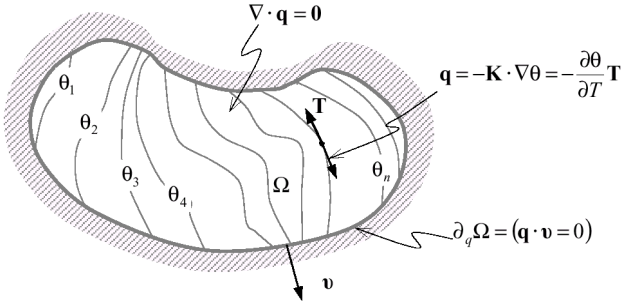

Figure 6. 2D algorithm to compute the envelopes of the propagation field as the isothermal lines for a heat conduction problem.

Such a type of global algorithms, although involving a (on the other hand very simple) multifield problem, appears suitable for dealing with multiple cracks and 3D problems.

2 MULTIPLE CRACKING TREATMENT

Cracking in plain and reinforced concrete often exhibits multiple cracks that grow separately but interacting to each other. Those cracks could be roughly classified into:

- *Primary cracks*, that grow along a relevant part of the deformation process and substantially contribute to the whole dissipation of the structure.

- *Secondary cracks*, that are active only for little range of the deformation process and consume a small amount of energy.

Even if secondary cracks are neglected, it is often observed in concrete the presence of several primary cracks during relevant parts of the deformation process. Moreover, for the ideal model that supplies the equilibrium paths in the action-response solutions space, any of the possible combinations in terms of activation or arrest of those cracks, determines a possible equilibrium path emanating as a bifurcated branch from the fundamental one (see Figure 7, left). Upon these circumstances numerical simulation becomes highly difficult and cumbersome and makes the general theoretical problem almost intractable.

However, experimentally observed cracking in concrete suggests that there exist a physical preference for some of those combinations that determines the actual crack pattern. This preference should be translated into a physical principle *or fundamental law that determines the path that will actually be followed* (Bazant&Cedolin 1991, pp. 650).

For adiabatic (slow) deformation processes this principle turns out to be the *maximum dissipation principle* which translates into the *maximum second order work for load control* and the *minimum second order work for displacement control* (Bazant&Cedolin 1991, pp. 658).

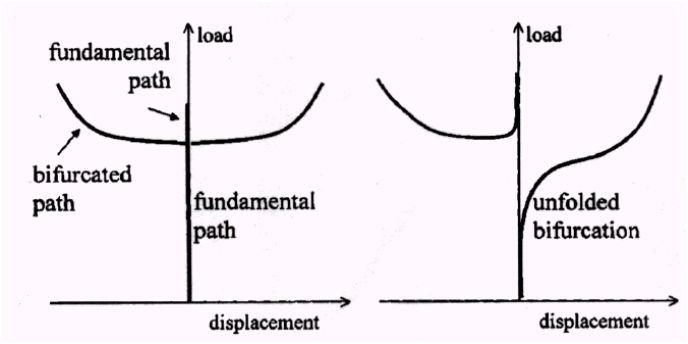

Figure 7. (from Gastebled et al. 2000): Bifurcation unfolding. Left: unperturbed solution. Right: perturbed solution

2.1 *Bifurcation unfolding*

For practical purposes in numerical simulation the maximum dissipation criterion does not avoid the heavy task of carrying out a bifurcation analysis and search for the most dissipative evolution of the cracking at every time step of the analysis (Gastebled et al. 2000). On the other hand, one could resort to perturbation techniques to unfold the bifurcation in the solution space and, therefore, assure a unique stable path (see Figure 7, right). The problem there is that the type of perturbation determines, in turn, the type of unfolding and, thus, the obtained solution (imperfection sensitive solution).

However, one could *postulate* a type of perturbation to produce the correct unfolding according to the criterion above. The physical meaning and experimental fitting of the obtained numerical results would then assess the correctness of that assumption. This is the procedure, based on a *discrete viscous perturbation at the crack path,* which will be described in next sections.

2.2 *Discrete viscous perturbation in the crack path*

2.2.1 *Symmetric formulation*

Nodal enrichment presented in section 1.3.2 can be cast into the following variational setting:

Let us consider the boundary value problem on the solid Ω sketched in Figure 8, exhibiting a strong discontinuity $[\![\mathbf{u}]\!]$at the discontinuity path S, and the corresponding virtual work principle:

$$\underbrace{\int_\Omega \boldsymbol{\sigma} : \underbrace{\nabla^S \boldsymbol{\eta}}_{\delta\boldsymbol{\varepsilon}}\, dV}_{\substack{\text{Internal Virtual}\\ \text{Work } (\delta\mathbb{W}^{\text{int}})}} = \underbrace{\int_\Omega \mathbf{b}\cdot\underbrace{\boldsymbol{\eta}}_{\delta\mathbf{u}}\, dV + \int_{\Gamma_\sigma} \mathbf{t}^*\cdot\underbrace{\boldsymbol{\eta}}_{\delta\mathbf{u}}\, d\Gamma}_{\substack{\text{External Virtual}\\ \text{Work } (\delta\mathbb{W}^{ext})}} \quad \forall \boldsymbol{\eta}\in\mathbb{V} \tag{12}$$

where $\mathbb{V}$ stands for the space of, kinematically admissible, virtual displacements:

$$\mathbb{V} := \{\boldsymbol{\eta}(\mathbf{x}) = \overline{\boldsymbol{\eta}} + H_S\widetilde{\boldsymbol{\eta}} \,|\, \overline{\boldsymbol{\eta}}(\mathbf{x})\big|_{\mathbf{x}\in\Gamma_u} = \widetilde{\boldsymbol{\eta}}(\mathbf{x})\big|_{\mathbf{x}\in\Gamma_u} = \mathbf{0}\} \tag{13}$$

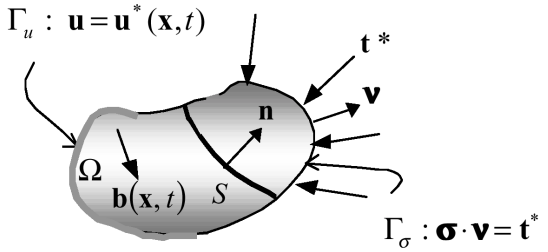

Figure 8. Boundary value problem

Some algebraic manipulations show that the Euler-Lagrange equations fot the variational principle (12) are:

$$\nabla\cdot\boldsymbol{\sigma} + \mathbf{b} = \mathbf{0} \quad \text{in } \Omega / S \rightarrow \text{momentum balance} \tag{14}$$

$$\boldsymbol{\sigma}\cdot\boldsymbol{\nu} - \mathbf{t}^* = \mathbf{0} \quad \text{in } \Gamma_\sigma \rightarrow \text{prescribed tractions} \tag{15}$$

$$\boldsymbol{\sigma}^{-}_{\Omega/S}\cdot\mathbf{n}-\boldsymbol{\sigma}^{+}_{\Omega/S}\cdot\mathbf{n}=\mathbf{0}\ \text{ in } S\rightarrow\begin{cases}\text{outer traction}\\ \text{continuity}\end{cases}\qquad(16)$$

$$\boldsymbol{\sigma}_{S}\cdot\mathbf{n}-\boldsymbol{\sigma}^{+}_{\Omega/S}\cdot\mathbf{n}=\mathbf{0}\ \text{ in } S\rightarrow\begin{cases}\text{inner traction}\\ \text{continuity}\end{cases}\qquad(17)$$

Let us now consider a *perturbed problem* characterized by the addition of a set of viscous surface forces $\tilde{\mathbf{t}}(\mathbf{x},t)$, at the discontinuity interface S, given by:

$$\tilde{\mathbf{t}}(\mathbf{x},t)=\bar{\gamma}[\![\dot{\mathbf{u}}]\!](\mathbf{x},t)\quad\forall\mathbf{x}\in S\qquad(18)$$

where $\bar{\gamma}>0$ is a perturbing (very small) viscosity and the upper dot stands for time (or pseudo time) derivative. The virtual work principle (12) reads now:

$$\underbrace{\int_{\Omega}\boldsymbol{\sigma}:\nabla^{S}\boldsymbol{\eta}\,dV}_{\text{Internal Virtual Work}}=\underbrace{\int_{\Omega}\mathbf{b}\cdot\boldsymbol{\eta}\,dV+\int_{\Gamma_{\sigma}}\mathbf{t}^{*}\cdot\boldsymbol{\eta}\,d\Gamma+\int_{S}\underbrace{\bar{\gamma}[\![\dot{\mathbf{u}}]\!]}_{\tilde{\mathbf{t}}}\cdot\boldsymbol{\eta}\,dS}_{\text{External Virtual Work}}\qquad(19)$$
$$\forall\boldsymbol{\eta}\in\mathbb{V}$$

and the corresponding Euler-Lagrange equations are:

$$\nabla\cdot\boldsymbol{\sigma}+\mathbf{b}=\mathbf{0}\ \text{ in }\Omega/S\rightarrow\text{momentum balance}\qquad(20)$$

$$\boldsymbol{\sigma}\cdot\boldsymbol{\nu}-\mathbf{t}^{*}=\mathbf{0}\ \text{ in }\Gamma_{\sigma}\rightarrow\text{prescribed tractions}\qquad(21)$$

$$\boldsymbol{\sigma}^{-}_{\Omega\setminus S}\cdot\mathbf{n}-\boldsymbol{\sigma}^{+}_{\Omega\setminus S}\cdot\mathbf{n}=\bar{\gamma}[\![\dot{\mathbf{u}}]\!]\ \text{ in } S\rightarrow\begin{cases}\text{perturbed}\\ \text{outer traction}\\ \text{continuity}\end{cases}\qquad(22)$$

$$\boldsymbol{\sigma}_{S}\cdot\mathbf{n}-\boldsymbol{\sigma}^{+}_{\Omega\setminus S}\cdot\mathbf{n}=\bar{\gamma}[\![\dot{\mathbf{u}}]\!]\ \text{ in } S\rightarrow\begin{cases}\text{perturbed}\\ \text{inner traction}\\ \text{continuity}\end{cases}\qquad(23)$$

From equations (14) to (23) it appears that, as the viscosity $\bar{\gamma}$ tends to zero, the original problem is recovered. However the introduction of the viscous perturbation $\bar{\gamma}$ has a relevant consequence on the uniqueness of the problem. In fact, let us consider two possible solutions whose differences, in terms of the displacements, strains and stresses at a given time t, are respectively: $\Delta\mathbf{u}(t)$, $\Delta[\![\mathbf{u}]\!](t)$, $\Delta\boldsymbol{\varepsilon}(t)$ and $\Delta\boldsymbol{\sigma}(t)$, which satisfy (from subtraction of equation (19) for both solutions):

$$\int_{\Omega}\Delta\boldsymbol{\sigma}:\nabla^{S}(\boldsymbol{\eta})dV-\int_{S}\bar{\gamma}\Delta[\![\dot{\mathbf{u}}]\!]\cdot\boldsymbol{\eta}dS\,dV=0\quad\forall\boldsymbol{\eta}\in\mathbb{V}\qquad(24)$$

Let us now consider the *bifurcation time* t_B where a bifurcation, *in terms of different combinations of arrest/activation of cracks*, takes place. This means that there are (at least) two possible solutions in terms of the *jump evolution* at S:

$$[\![\dot{\mathbf{u}}]\!]^{(1)}(\mathbf{x}_S,t_B)\neq[\![\dot{\mathbf{u}}]\!]^{(2)}(\mathbf{x}_S,t_B)\text{ for some }\mathbf{x}_S\in S$$
$$\Delta[\![\dot{\mathbf{u}}]\!](\mathbf{x}_S,t_B)=[\![\dot{\mathbf{u}}]\!]^{(2)}-[\![\dot{\mathbf{u}}]\!]^{(1)}\neq\mathbf{0}\text{ for some }\mathbf{x}_S\in S\qquad(25)$$

emerging from the same fundamental branch at t_B, and, therefore,

$$\Delta\mathbf{u}(t_B)=\Delta\boldsymbol{\varepsilon}(t_B)=\Delta\boldsymbol{\sigma}(t_B)=\mathbf{0}\qquad(26)$$

Inserting now equation (26) into equation (24)and for the particular choice $\boldsymbol{\eta}(\mathbf{x})\equiv\Delta[\![\dot{\mathbf{u}}]\!](\mathbf{x},t_B)\in\mathbb{V}$ one can write:

$$\int_{S}\bar{\gamma}\Delta[\![\dot{\mathbf{u}}]\!]\cdot\Delta[\![\dot{\mathbf{u}}]\!]dS=\int_{S}\bar{\gamma}\|\Delta[\![\dot{\mathbf{u}}]\!]\|^{2}dS=0\qquad(27)$$

and, therefore,

$$\Delta[\![\dot{\mathbf{u}}]\!](\mathbf{x},t_B)=\mathbf{0}\quad\forall\mathbf{x}\in S\qquad(28)$$

Which is in contradiction with equation (25) and, in consequence, *all bifurcations in terms of different combinations of crack arrest/activation are precluded*. This states the beneficial effects of the discrete viscous perturbation (18) in unfolding that type of bifurcations.

2.2.2 *Unsymmetric formulation*

Some types of finite element formulations (the so-called statically and kinematically optimal formulations (Oliver 1996, Armero&Garikipati 1996), belonging to the family of elemental enrichment discussed in section 1.3.1, can not be cast into a complete Galerkin type setting. In these formulations, the inner traction continuity equation (17) is locally weighted.

In this case the viscous perturbation can be directly introduced in that equation under the form of equation (23). Then, by subtracting two possible solutions inserted in this equation one can write:

$$\Delta\boldsymbol{\sigma}_{S}(\mathbf{x},t)\cdot\mathbf{n}-\Delta\boldsymbol{\sigma}^{+}_{\Omega\setminus S}(\mathbf{x},t)\cdot\mathbf{n}=\bar{\gamma}\,\Delta[\![\dot{\mathbf{u}}]\!](\mathbf{x},t)\ \text{ in } S\qquad(29)$$

and, since at the bifurcation time t_B:

$$\Delta\boldsymbol{\sigma}^{+}_{\Omega\setminus S}(\mathbf{x},t_B)=\Delta\boldsymbol{\sigma}_{S}(\mathbf{x},t_B)\cdot\mathbf{n}=\mathbf{0}\quad\forall\mathbf{x}\in S\qquad(30)$$

$$\Delta[\![\dot{\mathbf{u}}]\!](\mathbf{x}_S,t_B)\neq\mathbf{0}\text{ for some }\mathbf{x}_S\in S\qquad(31)$$

substituting equation (31) into equation (29) for $t=t_B$ one gets:

$$\bar{\gamma}\,\Delta[\![\dot{\mathbf{u}}]\!](\mathbf{x},t_B)=\mathbf{0}\quad\forall\mathbf{x}\in S\qquad(32)$$

which, for $\bar{\gamma}\neq0$, contradicts equation (31) this precluding any bifurcation of the considered type. Therefore the same benefits, to unfold crack opening/arrest bifurcations, than in the variationally consistent case should be expected.

2.2.3 *Time stepping. Critical time step*

In the context of a time (or pseudo-time) advancing algorithm, since progression along the equilibrium path in the action-response space is discrete, it is not possible to guarantee (for a given length of the time step $\ell_t(\Delta t)$) the uniqueness of the algorithmic response for the unfolded problem (see Figure 9). However it is possible to determine the critical length of the time step $\ell_t^{crit}(\Delta t^{crit})$ to assure algorithmic uniqueness.

Let us consider the space-time discretized version of the problem, in rate version for the elemental enrichment case of section 1.3.1, at time $t+\Delta t$:

$$\underbrace{\begin{bmatrix} \mathbf{K}_{dd} & \mathbf{K}_{d\alpha} \\ \mathbf{K}_{\alpha d} & \mathbf{K}_{\alpha\alpha} \end{bmatrix}}_{\mathbf{K}_{t+\Delta t}} \underbrace{\begin{bmatrix} \dot{\mathbf{d}}_{t+\Delta t} \\ \dot{\boldsymbol{\alpha}}_{t+\Delta t} \end{bmatrix}}_{\dot{\mathbf{a}}_{t+\Delta t}} = \underbrace{\begin{bmatrix} \dot{\mathbf{f}}_{t+\Delta t} \\ \mathbf{0} \end{bmatrix}}_{\dot{\mathbf{F}}_{t+\Delta t}} \tag{33}$$

where $\mathbf{d}$ stands for the regular (nodal) degrees of freedom and $\boldsymbol{\alpha} = \lfloor \boldsymbol{\alpha}^{(1)}, \boldsymbol{\alpha}^{(1)} .... \boldsymbol{\alpha}^{(n)} \rfloor^t$ are the internal degrees of freedom corresponding to the n enriched (crossed by the cracks) elements. The corresponding perturbed problem according to equation (23) reads:

$$\underbrace{\begin{bmatrix} \mathbf{K}_{dd} & \mathbf{K}_{d\alpha} \\ \mathbf{K}_{\alpha d} & \mathbf{K}_{\alpha\alpha} + \dfrac{\bar{\gamma}}{\Delta t}\mathbf{1} \end{bmatrix}}_{\tilde{\mathbf{K}}_{t+\Delta t}} \underbrace{\begin{bmatrix} \dot{\mathbf{d}}_{t+\Delta t} \\ \dot{\boldsymbol{\alpha}}_{t+\Delta t} \end{bmatrix}}_{\dot{\mathbf{a}}_{t+\Delta t}} = \underbrace{\begin{bmatrix} \dot{\mathbf{f}}_{t+\Delta t} \\ \dfrac{\bar{\gamma}}{\Delta t}\dot{\boldsymbol{\alpha}}_{t} \end{bmatrix}}_{\dot{\mathbf{F}}_{t+\Delta t}} \tag{34}$$

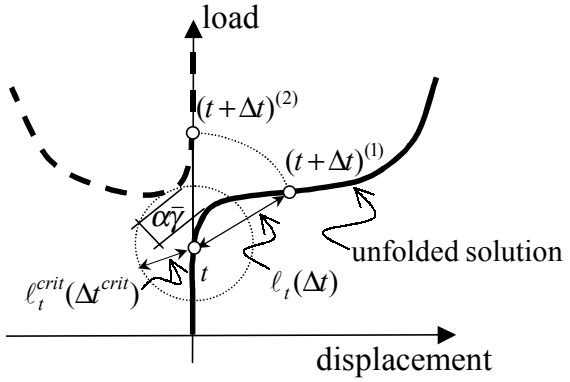

Figure 9. Algorithmic bifurcation for the unfolded problem. For $\ell_t(\Delta t) > \ell_t^{crit}(\Delta t^{crit})$ the algorithmic solution may not be unique.

A non-unique solution at time $t+\Delta t$ is characterized by the existence of several solutions $\dot{\mathbf{a}}_{t+\Delta t}^{(i)}\ i = 1,2..$ for equation (34) whose differences $\Delta\dot{\mathbf{a}}_{t+\Delta t} \neq \mathbf{0}$ fulfill:

$$\tilde{\mathbf{K}}_{t+\Delta t} \cdot \Delta\dot{\mathbf{a}}_{t+\Delta t} = \mathbf{0} \tag{35}$$

and pre-multiplying times $\Delta\dot{\mathbf{a}}_{t+\Delta t}$:

$$\Delta\dot{\mathbf{a}}_{t+\Delta t} \cdot \tilde{\mathbf{K}}_{t+\Delta t} \cdot \Delta\dot{\mathbf{a}}_{t+\Delta t} = 0 \tag{36}$$

which states the singularity of $\tilde{\mathbf{K}}_{t+\Delta t}$. Therefore, that value of $\Delta t = \Delta t^{crit}$ that guarantees positive definiteness of $\tilde{\mathbf{K}}_{t+\Delta t}$ precludes any bifurcation. Since sub-matrix $\mathbf{K}_{dd}$ in equation (34) can be shown to be positive, an approximate value of Δt^{crit} can be obtained by imposing positive definiteness of the symmetric part of all the diagonal sub-matrices associated to the enriching degrees of freedom $\boldsymbol{\alpha}$, i.e.:

$$symm(\mathbf{K}_{\alpha\alpha}^{(e)}) + \frac{\bar{\gamma}}{\Delta t}\mathbf{1} \rightarrow \text{positive def.}\ \forall e \in \{1,2..n_e\} \tag{37}$$

or, equivalently,

$$\lambda_{min}^{sym^{(e)}} + \frac{\bar{\gamma}}{\Delta t} > 0 \ \ \forall e \in \{1,2...n_e\} \tag{38}$$

where $\lambda_{min}^{symm^{(e)}}$ stands for the minimum eigenvalue of $symm(\mathbf{K}_{\alpha\alpha}^{(e)})$. From equation (38) the following value for Δ^{crit} emerges:

$$\Delta^{crit} = \min_e \left(\frac{\bar{\gamma}}{< -\lambda_{min}^{symm^{(e)}} >}\right) \qquad \forall e \in \{1,2..n_e\} \tag{39}$$

where $< \bullet >$ stands for the ramp function.

2.3 *Crack shielding*

In the context of multiple cracks propagating in a real concrete structure it is barely observed two *active primary cracks* crossing each other. However this is a case that can occur during the non-linear iterative procedure in the numerical model unless this possibility is precluded. Besides, if the finite element is not designed to bear multiple cracks this can result in a sort of numerical locking and a subsequent loss of convergence. To circumvent this problem, in the numerical examples presented below the elements inside a *shielding zone* (whose width is defined by the user) around an existing propagating crack can not be crossed by any external crack (see Figure 13). This prevents the formation of a number of spurious secondary cracks, around the primary ones, that give rise to numerical difficulties but do not provide any gain in the physical insight of the problem.

3 NUMERICAL SIMULATIONS

The modeling scheme outlined in previous sections has been implemented in a general multipurpose finite element code (Cervera et al. 2001). It has been used to simulate 2D fracture problems in concrete involving the onset and propagation of several primary cracks. A continuum damage model equipped with linear and exponential strain softening (Oliver, 2000), regularized according to equation (6), has been chosen to model the tensile cracking. Here, the material model is slightly modified, by precluding damage evolution whenever the principal stresses are negative, which avoid the material degradation in compressive stress states as should be expected in concrete.

Triangular and quadrilateral finite elements with elemental enrichment have been considered.

3.1 *Double notched four points bending test*

The four-point bending test shown in Figure 10, on a concrete specimen, has been analyzed by using a plane stress conditions.

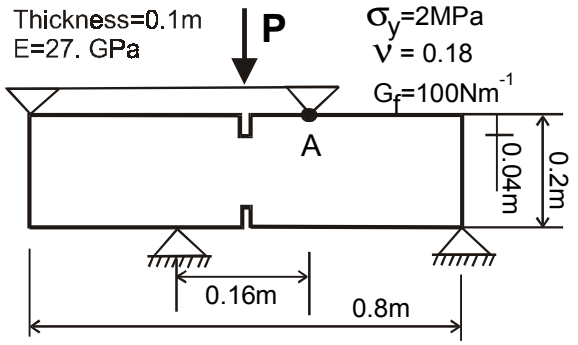

Figure 10. Four-point bending test for a double-notched beam, E: Young' modulus, ν: Poisson's ratio, σ_y: tensile strength. G_f: fracture energy

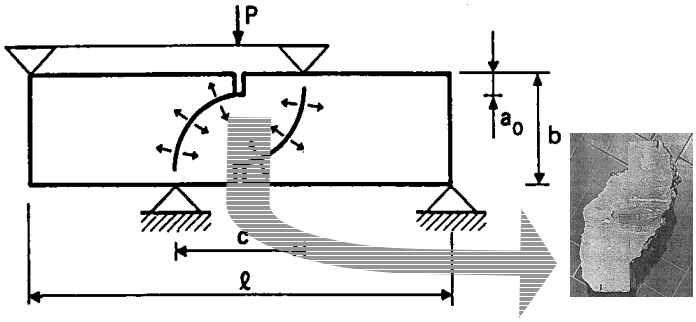

Figure 11. (from Bocca P., Carpintieri A., Valente S., 1991) Four-point bending test for a double-notched beam, Left: observed cracks. Right: detail of the concrete specimen between cracks after the test.

The experiment corresponds to one of the tests carried out by Bocca et al. (1991), who particularly remarked the mixed mode fracture character of the crack opening mode. They observed that the structure collapsed due two the formation of two primary cracks as displayed in Figure 11. The experimental critical load was 34460 N, lower than the one obtained by numerical simulation adopting a linear softening law for the damage model (Figure 12).

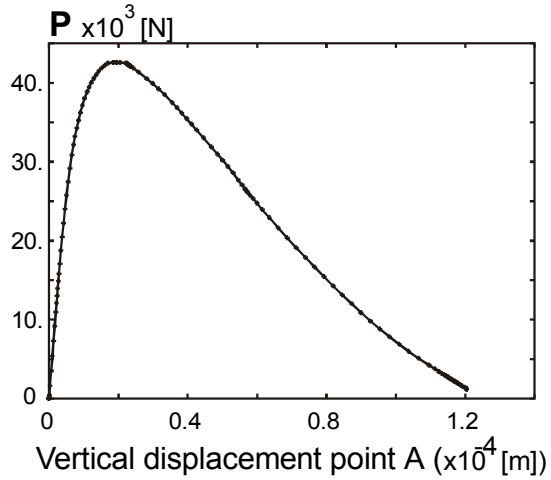

Figure 12. Load vs. vertical displacement of point A for the four point bending test.

In Figure 13, the crack pattern obtained at different steps of the analysis is shown. The black regions correspond to the shielding zone where crack propagation is forbidden. Every new crack sets its own shielding zone.

Two primary symmetric cracks are observed to propagate from the roots (at the notches) toward the load application points. These curves are in agreement with the experimental results.

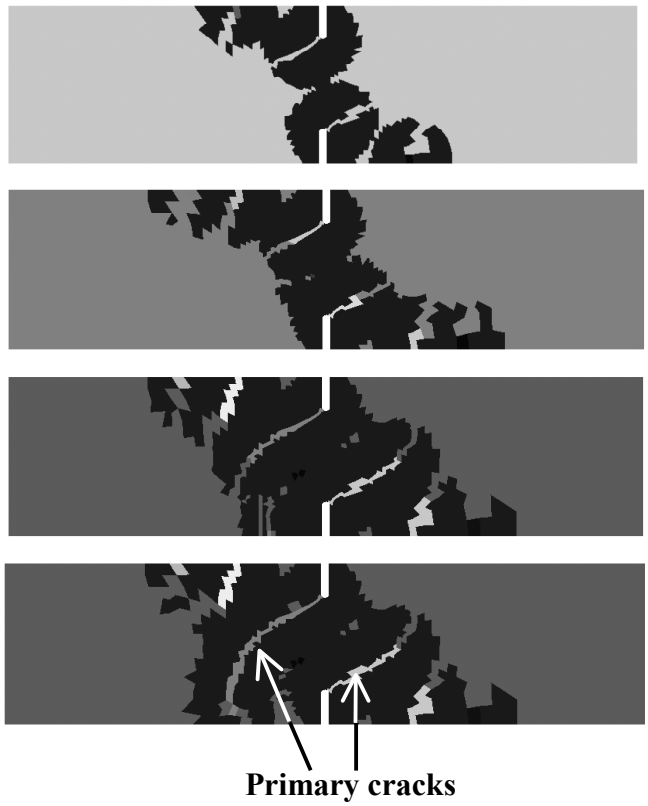

Figure 13. Double notched beam. From top to bottom: evolution of the crack pattern (elements crossed by the cracks are highlighted in gray. Black area around the crack paths corresponds to the shielding zone)

Figure 14 shows the active (opening) crack pattern for different steps of the analysis. A white line means that the crack is opening, in contrast with the arrested cracks, which are not signaled. At initial stages, before the limit load is reached, it is observed that several cracks, both primary and secondary, are opening. After the peak load stage, only one of the primary cracks remains active. This fact states the presence of a bifurcation point, in the equilibrium curve of the perfect structure (at the peak of the load-displacement curve in Figure 12), and the fundamental path (corresponding to two active cracks) is unfolded by the viscous perturbation method described in section 2.2 into a one-active-crack path. Any numerical perturbation (introduced for instance by the finite element mesh) will select which one of the two primary cracks is remaining active.

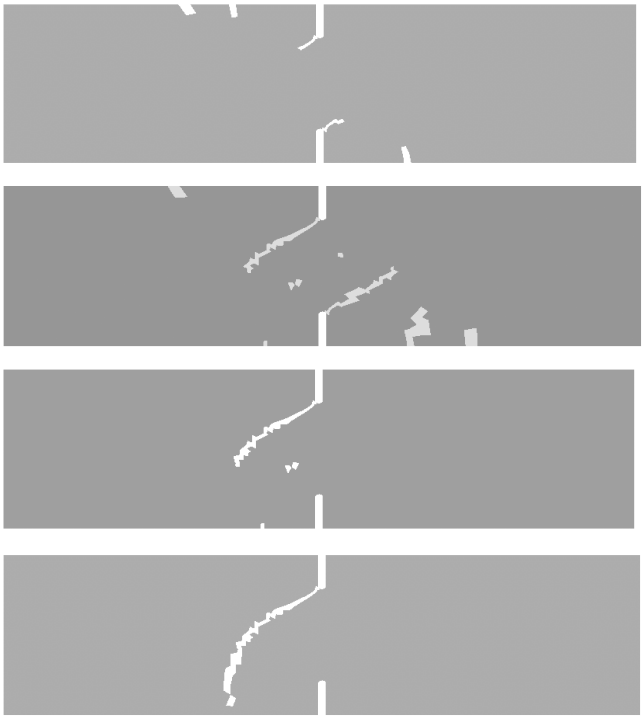

Figure 14. Double notched beam. From top to bottom: evolution of the active cracks for increasing times of the analysis (elements crossed by the active cracks are highlighted in white. The second and third pictures correspond, respectively, to load levels before and after the peak load).

3.2 *Steel slab debonding from a concrete specimen*

Next example corresponds to the simulation of the debonding of a steel slab from a concrete bulk by stretching the slab from both ends as it is shown in Figure 15.

This problem is an adaptation, to the plane strain case, of a rebar debonding axisymmetric problem presented in Rots (1988). Although the problem is not exactly the same in both cases, since the geometrical dimensions and material constants are the same one should expect similar results for the structural behavior and crack pattern.

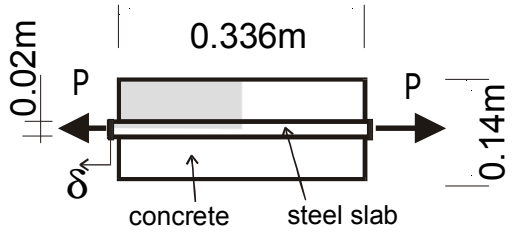

Figure 15. Debonding of a steel slab from a concrete block in plane strain. The discrete model corresponds to a quarter of the structure.

The bond-slip mechanism that rules the transmission of the tangential stresses to the concrete is modeled by a thin layer of an ideally plastic material (J2 plasticity) at the steel-concrete interface (see Figure 16). The stiffness of this bonding material is equal to that of the steel slab. The concrete is modeled in a similar way than in the previous example. The material properties (Young' modulus, E_c, Poisson's ratio, ν_c, tensile strength, σ_c, and fracture energy, G_f) of concrete, as well as steel parameters and the yield stress, σ_{yb}, of the bounding material are displayed in Figure 16. Two different finite element meshes A (coarse) and B (fine) have been used for the numerical simulations.

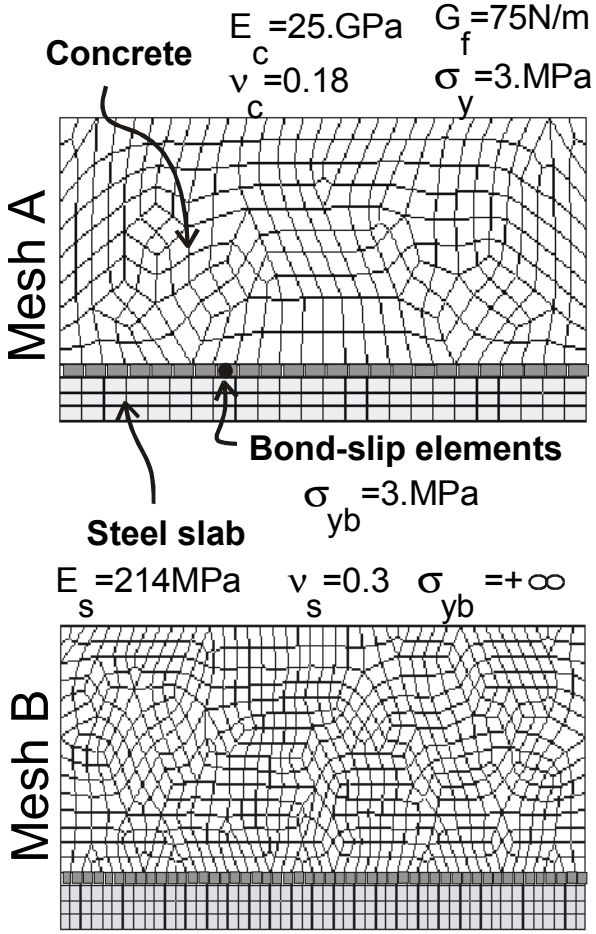

Figure 16. Steel slab in a concrete block. Finite element meshes.

Figure 17-(a) shows the evolution of the load P, applied at the end-face of the steel slab, vs. the displacement at the same point. In Figure 17-(b) it is shown, in detail, the typical snap-back behavior of this type of structures, for both meshes.

Secondary transverse cracks can be observed in an initial diffuse failure stage, before the snap-back of the equilibrium path takes place (see Figure 18-(a)). They initially nucleate at the end-face of the specimen but, as the loading increases, they spread out through the total steel-concrete interface length. An initial primary crack onsets and propagates along the concrete section, up to the complete softening of the material in that region (see Figure 18-(b)). The subsequent loss of structural loading capacity then triggers the severe snap-back displayed in the equilibrium path in Figure 17.

At this stage, the structure is still able to hold an increasing external loading transmitted through the steel slab to other sections of the concrete bulk. In fact, a subsequent loading after the snap-back in-

duces the propagation of a second primary crack (see Figure 18-(c)) across the concrete.

Finally, Figure 19 shows the corresponding deformed meshes.

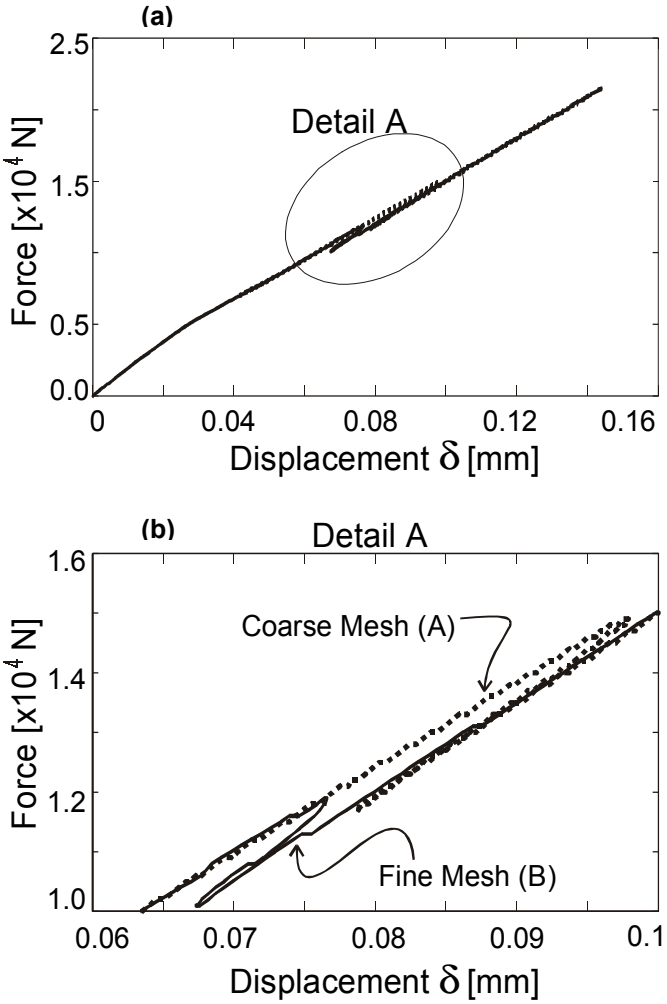

Figure 17. Steel slab in a concrete block; (a) Load vs. displacement curve at the end-face of the slab; (b) detail of the curve showing the snap-back caused by the complete softening of the primary crack.

4 CONCLUDING REMARKS

Along this work different ingredients to model multiple cracking in concrete structures by resorting to the strong discontinuity approach have been tackled. The resulting methodology endows the numerical simulation of cracking of concrete some interesting features, i.e.:

- A clear connection of the continuum format simulation with a discrete one based on Fracture Mechanics settings.
- The same (continuum) non-linear constitutive model is used to model both the damage at the uncracked concrete and the decohesion at the crack interface.
- Finite elements with embedded discontinuities are completely insensitive to mesh size and alignment.
- The model can deal with multiple cracks simultaneously progressing through the body and to unfold the possible bifurcations due to multiple crack arrest/activation.

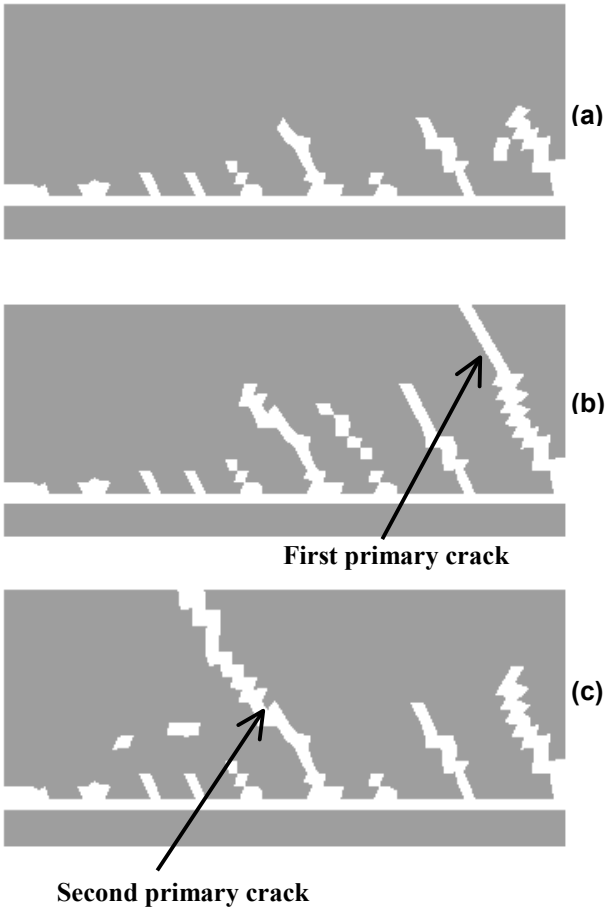

Figure 18. Steel slab in a concrete block. From (a) to (c): evolution of the active cracks for increasing times of the analysis (a) at an initial stage, (b) before the snap-back point and (c) after the snap-back point (elements crossed by the active cracks are highlighted in white).

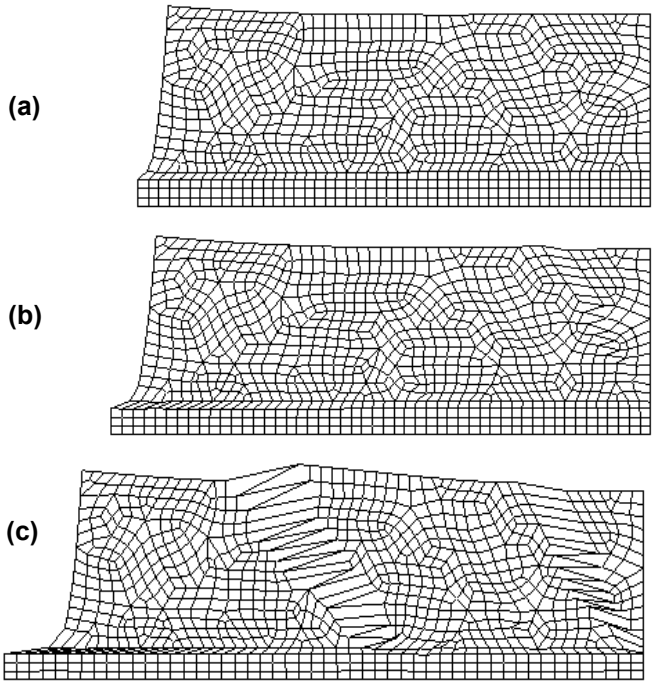

Figure 19. Steel slab in a concrete block. From (a) to (c): Deformed (amplified) meshes at identical times than in Figure 18.

ACKNOWLEDGMENTS

This work has been done with support of the Spanish Ministry of Science and Technology under grants MAT-2001-3863-C03-03 and MAT-2000-0436. This support is gratefully acknowledged.

REFERENCES

Armero F. and Garikipati K., 1996, An analysis of strong discontinuities in multiplicative finite strain plasticity and their relation with the numerical simulation of strain localization in solids, *Int.J. Solids and Structures* (33): 2863-2885

Bazant Z.P., Cedolin L.,1991, *Stability of Structures*, Oxford University Press

Bazant Z.P., Planas J., 1998. *Fracture and size effect in concrete and other quasibrittle materials*, CRC Press.

Bocca P., Carpintieri A., Valente S., 1991, Mixed Mode Fracture of Concrete*, International J. of Solids & Structures* 27, (9), 1139-1153.

Cervera M., Agelet de Saracibar C., Chiumenti M.., 2001, COMET: a multipurpose finite element code for numerical analysis in solid mechanics. Technical University of Catalonia (UPC)

Gastebled O.J., May I.M., 2000, Bifurcation in the numerical solution of softening mechanisms, *Computers and Structures*, (78): 745-755

Oliver J., 1996. Modeling strong discontinuities in solid mechanics via strain softening constitutive equations. Part 2: Numerical simulation, *International Journal for Numerical Methods in Engineering*., (39):3601-3623

Oliver J., 2000. On the discrete constitutive models induced by strong discontinuity kinematics and continuum constitutive equations. *International Journal of Solids and Structures*, 37:7207-7229

Oliver J., Huespe A.E., Pulido M.D.G., Chaves E., 2001. From continuum mechanics to fracture mechanics: the strong discontinuity approach.. *Engineering Fracture Mechanics*, 69(2): 113-136

Oliver, J.; Huespe, A.E.; Samaniego, E.; Chaves, E.W.V.2002, On Strategies for Tracking Strong Discontinuities in Computational Failure Mechanics, *Proceedings of the Fifth World Congress on Computational Mechanics (WCCM V*), Editors: Mang, H.A.; Rammerstorfer, F.G.; Eberhardsteiner, J., Publisher: Vienna University of Technology, Austria, ISBN 3-9501554-0-6, http://wccm.tuwien.ac.at

Rots J.G., Computational modeling of Concrete Fracture, PhD Thesis, Delft University of Technology, September 1988.

Simó J.C., Oliver J., Armero F., 1993. An analysis of strong discontinuities induced by strain-softening in rate-independent inelastic solids. *Computational Mechanics* 12: 277-296

Wells G.N., Sluys L.J., 2001, A new method for modeling cohesive cracks using finite elements. *International Journal for Numerical Methods in Engineering* ,50,2667-2682}

Willam K. 2000, Constitutive models for engineering materials. *Encyclopedia of Physical Science & Technology* 3rd edition, Academic Press, New York, (3):603-633